Application of Stability Analysis of $Q(V)$-Characteristic Controls Related to the Converter-Driven Stability in Distribution Networks

Sebastian Krahmer, Stefan Ecklebe, Peter Schegner, *Senior Member, IEEE*, Klaus Röbenack

***Abstract*—As the amount of volatile, renewable energy sources in power distribution networks is increasing, the stability analysis of the latter is a vital aspect for network operators. Within the STABEEL project, the authors develop rules on how to parameterize the reactive power control of distributed energy resources to increase the performance while guaranteeing voltage stability. The work focuses on distribution networks with a high penetration of distributed energy resources equipped with $Q(V)$-characteristics. This contribution is based on the stability assessment of previous work and introduces a new approach utilizing the Circle Criterion. Herein, distributed energy resources can be modeled as detailed control loops or as approximations, derived from technical guidelines. In addition, the wavelet transform is applied to RMS time series simulations to obtain a more realistic, less conservative reference. With the aim of extending existing technical guidelines, the stability assessment methods are applied to various distribution networks.**

***Index Terms*—Converter-driven stability, power distribution control, Q(V), stability criteria, voltage control, voltage stability, volt/var**

I. Introduction

ACROSS Europe, a massive growth of distributed energy resources (DERs) based on wind and solar energy can be observed. These changes require not only an adaption of the existing electrical power networks but also of their operation in terms of voltage level control or reactive power provisioning. The network operators can meet these challenges by employing a combination of centralized and distributed voltage control concepts. One method of indirect voltage control is the $Q(V)$-control, which implements an adaption of the system reactive power depending on the voltage level at the network connection point with a $Q(V)$-characteristic [1]. Previous contributions show possible applications with regard to cost-effectiveness and efficiency [2]–[4], fallback voltage support [5] or optimal power flow [6] in distribution networks (DNs). However, all related operational strategies must meet stability requirements.

Possible interactions of $Q(V)$-characteristic controls are classified as (short-time) voltage stability or as *slow-interaction converter-driven stability*, newly introduced in [7]. Considering $Q(V)$-characteristic control, network codes, such as RfG [8], are very restrictive regarding parameterization limits, which counteract a more network-serving application. Therefore, controller interactions must continue to be investigated and an extended generic computation approach should be provided to distribution network operators (DSOs).

S. Krahmer and P. Schegner are with the Chair of Electrical Energy Supply at the TUD Dresden University of Technology, Dresden, Germany (email: sebastian.krahmer@tu-dresden.de)

S. Ecklebe and K. Röbenack are with the Instiute of Control Theory at the TUD Dresden University of Technology, Dresden, Germany

A. Relevant Literature

In response to the aforementioned challenges, several contributions on related stability aspects have been published, especially to low-voltage (LV) DNs. Aspects considered include instability at large controller dead times [9] and the influence of damping time constants [4], [10]. The authors of [11] analyze small-signal stability using the NYQUIST criterion, focusing on single-input single-output systems. They conclude that all dynamics in the same time domain must be considered for parameterization, while [12] explicitly states that faster voltage measurement and averaging leads to reduced stability margins. As [10] stated for DER dominated LV networks, there exist no (practically relevant) limitations using a $Q(V)$-characteristic based control for photovoltaic (PV) following fundamental parameterization rules. At higher voltage levels, single DERs are grouped together and then equipped with farm control. Different voltage control strategies ought to be considered: central [13] or decentral [3], [14]. Furthermore, a communication delay within farm control must be taken into account at this point [15]. Also, especially in weak networks the DSO must be aware of voltage control interactions, as shown in [16]–[18], where the latter discusses trade-offs between the plants local gains and the convergence rate of the system after an error.

However, the case of DERs directly connected to the medium (MV) and high voltage (HV) network with $Q(V)$-characteristic control, which differs from the above cases in terms of network topology and installed plant capacity, has been less studied so far. Due to this, a first stability assessment (SA) for MV and HV levels with focus on wind farm (WF) models is introduced in previous work [19]. This approach does not require knowledge of the control model parameters, but results in conservative thresholds, i. e. remains in parts below the network code recommendations. Further considerations about the modeling of nonlinear network feedback were carried out in [20]. Finally, the extended approach [21] for assessing converter-driven stability on the basis of time-discrete modeling and fixed-point iteration shows operating point independent but also moderate results.

Alternatively, with detailed knowledge of the system, an evaluation is possible with the aid of network calculation

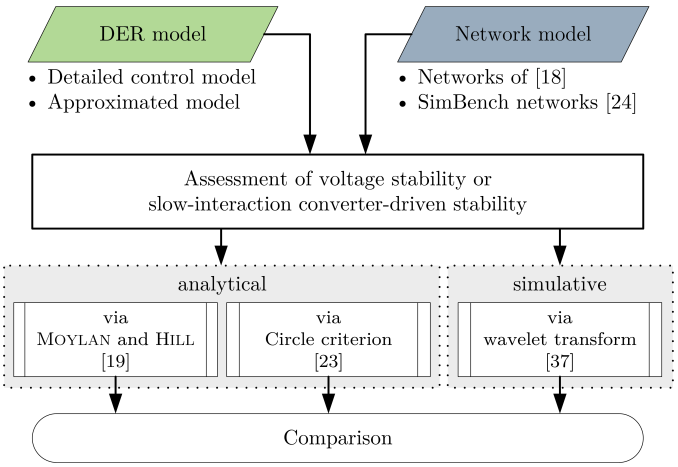

Fig. 1. Overview of the analytical and simulative stability assessment methods used in this paper and the input data required.

software such as DIgSILENT `PowerFactory`. In particular, an automated analysis of time series in the RMS time domain is possible using the wavelet transform, [22] gives an overview of various applications.

B. Contributions and Organization

The objective of this contribution is the application of procedures for SA. Thus, the authors deduce an analytically based criterion for the SA of interacting $Q(V)$-controlled DERs or voltage controllers in MV and HV networks. This novel approach is based on the so-called Circle Criterion, cf. [23, Ch. 7.1.1], and is characterized by a lower degree of conservatism compared to previous work [19]. Furthermore, in case of lack of information regarding specific DER models, PT_2 approximations with reduced complexity can be derived. Here we show that more accurate information about DER models results in better outcomes of the SA. Moreover, this contribution extends our recent work [1] by applying the wavelet transform to the SA based on simulations in the RMS time domain. The evaluation process is depicted in Fig. 1. The software implementation of this case study is available as a CodeOcean capsule [24].

The proposed work is organized as follows. Section II explores the power system modeling including DERs with $Q(V)$-characteristic. In Section III, the authors introduce various DER models, which can be expressed by detailed control loops or by approximated PT_2 models. Then, the SA of nonlinear systems utilizing the Circle Criterion is introduced in Section IV. In the next section, a posteriori SA of simulated or measured time series using the wavelet transform is presented and the application to voltage histories is discussed. In VI, the presented SA methods are applied to various HV benchmark networks, including a HV network from the SimBench project [25]. Finally, the results are compared with the findings of previous work [19] and RMS time domain simulations of detailed modeled systems. Final remarks and potential future developments are summarized in Section VII.

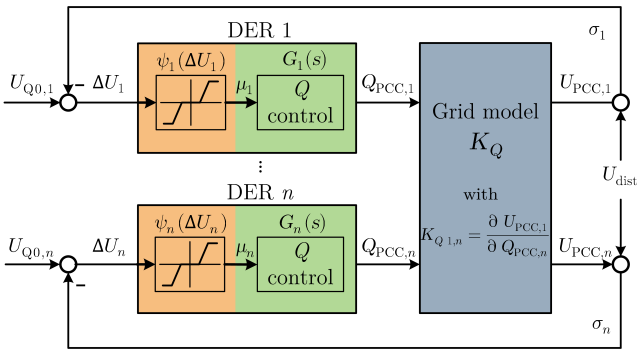

Fig. 2. Generic reactive power control path for MIMO case, adapted to a $Q(V)$-characteristic control.

II. System Model

This section provides a brief summary of the voltage control loop of $Q(V)$-controlled DERs. The complete control loop consists of the $Q(V)$-characteristic, which calculates a desired reactive power from the nodal voltage, which then, shaped by a plant-specific control loop, finally feeds a static linear network model, which in turn results in the new nodal voltage. Figure 2 shows this overall system model for the multiple-input multiple-output (MIMO) case assuming a DN with n $Q(V)$-controlled nodes. The components of the system are explained in more detail below.

A. Q(V)-Characteristic Curve

The $Q(V)$-characteristic is a nonlinear function that maps the measured nodal voltage at the point of common coupling U_{PCC} to a desired reactive power and is shown in Fig. 3. It exhibits areas of saturation as well as a deadband, between which it is monotonically increasing. As introduced in previous work [19] and depicted in Fig. 3, the nonlinear $Q(V)$-characteristic can be generally represented by a sector enclosing this $Q(V)$-curve $\psi(\Delta U)$ between two linear functions with slope α and β, respectively. Here, ΔU is the deviation of the measured voltage from the origin of the characteristic U_{Q0}, which is not necessarily the nominal voltage U_{nom}[1]. Using this approach, even characteristics with variable or optimized "curved" slopes m as well as asymmetric slopes can be taken into account. For the cases considered in this publication, the linear slope m is given as:

$$m := \frac{\Delta Q/P_{\mathrm{r}}}{\Delta U/U_{\mathrm{n}}} \text{ with } [m] = \frac{\%}{\mathrm{pu}}. \tag{1}$$

In the following, the $\psi(\Delta U)$ is bounded by the x-axis from below and by a linear function with slope $\beta > 0$ from above.

B. Static Network Model

Within this contribution, all DERs are assumed to be coupled through a common static network, modeled by the constant nodal voltage sensitivity matrix $\boldsymbol{K}_Q \in \mathbb{R}^{n\times n}$ [19]. For the calculation of this simplified network model, one have to establish the apparent power equations of the network and do

[1]To accurately represent this relation, all voltage variables in Fig. 3 are related to the nominal voltage and represented by $\tilde{(\cdot)}$.

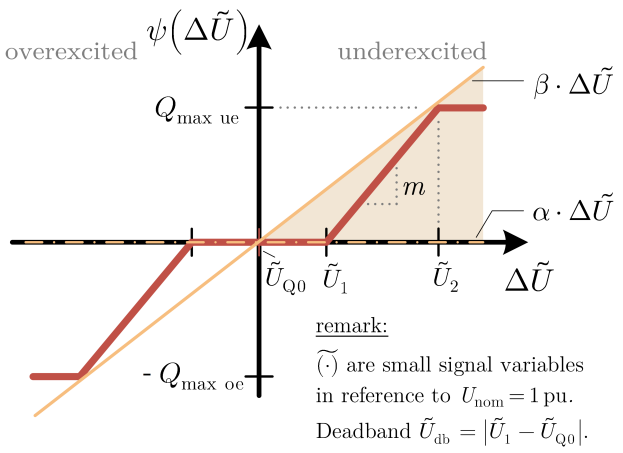

Fig. 3. $Q(V)$-characteristic $\psi(\Delta U)$ with an enclosing sector area.

some transformations. The complex apparent power in each network node can be calculated from the complex vector of line-to-ground nodal voltages $\underline{\boldsymbol{u}}$ via

$$\underline{\boldsymbol{s}} = 3\ \text{diag}\,\underline{\boldsymbol{u}}\,\underline{\boldsymbol{Y}}^*\underline{\boldsymbol{u}}^* = \boldsymbol{p} + \text{j}\boldsymbol{q}, \tag{2}$$

wherein $\underline{\boldsymbol{Y}}$ represents the node admittance matrix of the network.

For a given power system operating point, the JACOBIAN of the apparent power related to the complex voltage $\boldsymbol{J} \in \mathbb{R}^{2n\times 2n}$ can be obtained by linearization[2] using the node admittance matrix of the network $\underline{\boldsymbol{Y}}$ (2), see [26, Eq. 5.114]. The operating point is defined by complex nodal voltages corresponding to the distribution of active and reactive load power. Then, the nodal voltage sensitivity matrix $\boldsymbol{K}_Q$ can be obtained by inversion of $\boldsymbol{J}$ and subsequent selection of the submatrix with respect to the ith element definition $K_{Q\,i,i} = \frac{\partial U_i}{\partial Q_i}$, $i = 1,\ldots,n$, c. f. Fig. 2.

C. Multi-Input Multi-Output System Model

The underlying technology and operating mode of each DER have an impact on the reactive control path representation. However, assuming a normal operation mode and neglecting reactive power constraints at low active power infeed, the reactive power control path can be treated separately from the remaining plant model. As many different models can be used here, Section III will give a detailed overview of relevant plant models that are related to the DER technology or to a PT_2 representation, respectively. As depicted in Fig. 2, the reactive power control loop $G_i(s)$, $i = 1,\ldots,n$ of each plant can be separated from the nonlinear $Q(V)$-characteristic $\psi_i(\Delta U_i)$, $i = 1,\ldots,n$ regardless of the fashion in which the control is implemented inside of $G_i(s)$.

Subsequently, defining the input vector $\boldsymbol{\mu}(s) := (\mu_1(s),\ldots,\mu_n(s))^\top \in \mathbb{R}^n$ and output vector $\boldsymbol{\sigma}(s) := (\sigma_1(s),\ldots,\sigma_n(s))^\top \in \mathbb{R}^n$ as well as pooling the independent transfer functions in $\boldsymbol{G}(s) := \text{diag}\,G_1(s),\ldots,G_n(s)$, the system dynamics can be written as

$$\boldsymbol{\sigma}(s) = \tilde{\boldsymbol{G}}(s)\boldsymbol{\mu}(s) \tag{3a}$$
$$\boldsymbol{\mu}(s) = \boldsymbol{\psi}(\boldsymbol{\sigma}(s)) \tag{3b}$$

(cf. Fig. 2 with $U_{\text{Q0},i} = U_{\text{dist}} = 0$) with the overall transfer function matrix $\tilde{\boldsymbol{G}}(s) := \boldsymbol{G}(s)\boldsymbol{K}_Q$.

As this contribution assumes balanced single-line network models, the presented approach would need to be extended for unbalanced networks. Additionally, a more realistic, i. e. voltage dependent network model is presented in [20] by including the derivative of $\boldsymbol{K}_Q(\Delta U)$, but is not used in this contribution, since it adds an additional nonlinearity. In this respect, an alternative time-discrete modeling approach is discussed in [21].

III. PLANT MODELS

In this section, we summarize different DER models $G(s)$ from the literature and integrate them into the system model of (3). Furthermore, for cases where neither the model parameters nor the detailed model structure are known, two alternative approaches are presented, referred to as PT_2-DER and PT_2-TAR. The first approach assumes that the DER operator does not supply a detailed model to the stability assessor, but provides a model approximation, e. g. in form of a PT_2-element. The second approach can be interpreted as a fallback, for the case that a detailed model or even an approximation based on this model is not available. Finally, a comparison is drawn on the example of a wind farm.

A. Detailed Models of Voltage Control in Distributed Energy Resources (Orig. DER)

Normative publications and research work such as [27]–[30] provide complex models of almost all different DER types. Furthermore, regarding the Q-control dynamics $G_i(s)$ the authors focus on three popular DER types: (i) WF of type fully rated converter (FRC), (ii) WF of type double fed induction generator (DFIG), (iii) photovoltaic farm (PVF), whose detailed models and parameterizations are given in Table III. Note that models of other reactive power resources such as static var or static synchronous compensators [31], [32] are not discussed in this contribution. In addition, battery storages are not explicitly considered here due to their widely adaptable inverter behavior.

All mentioned DER models can be extended by adding a farm control unit containing logic of the $Q(V)$-characteristic as well as additional measurements and delay blocks. The migration from individual unit control to farm control is characterized by an additional communication delay. This dead time block with the time constant T_g is set between the setpoint tracking Q_R and unit/inverter current control $\tilde{Q}_\text{set}$. Furthermore, a voltage-averaging block feeds into the $Q(V)$-characteristic, which further feeds into the reactive power control loop of the DER. However, as voltage-averaging has a gain of 1, the $Q(V)$-characteristic $\psi(\Delta U)$ can be swapped with it and combined with the downstream reactive power control loop [19]. Thus, one arrives at the summarized reactive power control loop $G(s)$ shown in Table III.

[2]For a more detailed consideration, please see [21].

B. PT_2-fit based on the Frequency Response of a specific DER Model (PT_2-DER)

Using the detailed DER model as fitting target, a realistic approximation can be provided by fitting a PT_2-element to the frequency response of a fully parameterized, detailed DER model. The PT_2-element is of the form:

$$G_{PT_2}(s) = \frac{1}{1 + 2DTs + T^2 s^2}. \tag{4}$$

The drawback is the required specification of DER model parameters, which, however, are usually provided to the DSO when the DER is commissioned. For this approach, the authors are using the frequency response with respect to magnitude and angle within a relevant frequency band for PT_2 fitting, as shown in Fig. 4a. This frequency band is derived from the expected bandwidth of the control loop inputs, as higher frequencies are filtered out in the previous layers. The lower bound can be defined by the transformer tap control and the upper bound can be set at twice the voltage averaging time constant. Therefore, for the PT_2 fit it follows that frequency f lies in the interval from $0.01\,\text{Hz}$ to $100\,\text{Hz}$.

Furthermore, the PT_2 static gain is fixed to 1 to match the static gain of the detailed model, cf. Fig. 4b. Table III shows the obtained PT_2 parameters.

C. PT_2-fit based on technical Guidelines (PT_2-TAR)

When connecting DERs to DNs, technical guidelines apply, which regulate, e. g., the way in which reactive power is provided [8]. Thus, specifications on the principle dynamics of reactive power provision are defined. The incorporation of these boundaries for a control response allows a reduction of model complexity toward a PT_2 representation.

The TAR [33] provides such a specification for the set of admissible control behaviors, by means of parameterization of a generic step response. The TAR specifies the three characteristic parameters maximum overshoot ξ, rise time to first reach $90\,\%$ of static gain $T_{90\%}$ as well as settling time T_{stl} to reach a tolerance band around the static gain. Assuming a "slow" parameterized DER, ξ is set to $15\,\%$, $T_{90\%} = 5\,\text{s}$ and T_{stl} should around $T_{90\%} + 3\,\text{s}$. An optimization algorithm based on least squares was used to fit a PT_2-element of (4). Thereby, the overshoot ξ, the rise time $T_{90\%}$ and the settling time T_{stl} are to be reproduced with only two degrees of freedom D, T, assuming that the static gain was set to 1 to match the static gain of the step response. As shown in Fig. 4b, a match of ξ and $T_{90\%}$ were weighted more significantly, because of the high impact on dynamic system response. Table III shows the obtained PT_2 parameters.

D. Comparison of Detailed and Approximated DER Models

Figure 4 shows the comparison of frequency and step responses of a detailed DER model with its PT_2 approximations. A WF-FRC model was used in this paper, cf. Table III (i).

The evaluation of the frequency response in Fig. 4a shows that PT_2-DER hits the magnitude in a sufficient manner, but underestimates for higher frequencies. As a mitigation for this deficit, it can be considered that the largest time constant

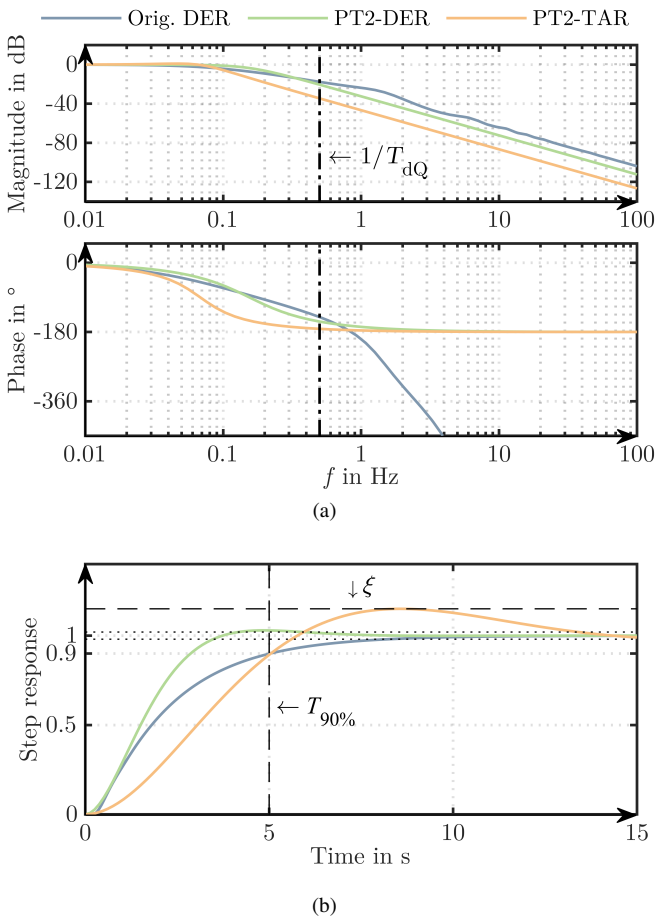

Fig. 4. Comparison of frequency and step responses of a detailed DER model (Orig. DER) with PT_2-approximations based on detailed DER model and generic TAR step response, respectively. A WF-FRC is used as DER model and the model parameterizations can be obtained from Table III. (a) Frequency response with kink frequency of the dominant DER PT1 element. (b) Step response with characteristic overshoot and rise time quantities.

in the DER control loop T_{dQ} significantly attenuates higher frequencies. In conclusion, adaptable PT_2 approximations can be used to safely emulate the original DER behavior in the relevant frequency range (left side of $1/T_{\text{dQ}}$ in Fig. 4a)

Figure 4b depicts the step responses, allowing the differences in the approximation to be determined. While the approximation based on TAR hits $T_{90\%}$ accurately, the overshoot ξ is assumed to be worse compared to the real DER model. In contrast, the approximation based on detailed DER has less $T_{90\%}$ and only slight overshoot ξ. This is to be expected since the approximation was performed in the frequency domain but is acceptable since the static gain is still achieved accurately and quickly. Thus, the estimation is conservative as it includes a more critical behavior.

IV. Stability Assessment of a Nonlinear MIMO System

Preliminary work [19] has introduced the stability criterion from Moylan & Hill to perform a stability assessment for systems with $Q(V)$-characteristic control which is conservative but can be employed without knowledge of specific DER transfer function $G(s)$. Assuming that the parameters of a DER

control $G(s)$ are known, different stability methods can be used now. Under the condition of a deterministic applicability, the so-called Circle Criterion is revisited in this section and its application to the system model (3) is discussed.

A. Stability criterion for DER MIMO system with Q(V)-characteristics

First, we introduce the concept of sector nonlinearities:

Definition 1 (Sector Nonlinearity, cf. [23, Def. 6.2])**.** *A (vector-valued) function $\boldsymbol{f} : \mathbb{R}^n \to \mathbb{R}^n$ is said to belong to the sector $[\mathbf{0}, \boldsymbol{K}]$ for a symmetric positive definite matrix $\boldsymbol{K} \in \mathbb{R}^{n\times n}$ if $\boldsymbol{f}(\boldsymbol{x})^\top (\boldsymbol{f}(\boldsymbol{x}) - \boldsymbol{K}\boldsymbol{x}) \leq 0$.*

Thus, if a function $\boldsymbol{f}(\boldsymbol{x})$ fulfills Definition 1 for a certain $\boldsymbol{K}$, we write $\boldsymbol{f}(\boldsymbol{x}) \in [\mathbf{0}, \boldsymbol{K}]$. Taking further into account the nature of the nonlinear $Q(V)$-characteristics $\psi_i(\Delta U_i)$ – as shown in Fig. 3 – we are able to formulate the following variant of the Circle Criterion:

Theorem 1 (Stability of a MIMO DER system with $Q(V)$-characteristics)**.** *The system* (3) *with the slope matrix $\boldsymbol{M} \coloneqq \operatorname{diag} \beta_1, \ldots, \beta_n$ is absolutely stable if $\boldsymbol{I} + \boldsymbol{M}\tilde{\boldsymbol{G}}(s)$ is strictly positive real.*

Proof. As every DER possesses its own local $Q(V)$-control, the static nonlinearity $\boldsymbol{\psi}(\Delta U)$ is decoupled, i. e. $\mu_i = \psi_i(-\sigma_i)$ holds for $i = 1, ..., n$. Thus, $\psi_i(\Delta U_i) \in [0, \beta_i]$ by Definition 1 and consequently $\boldsymbol{\psi}(\Delta U) \in [\mathbf{0}, \boldsymbol{K}]$ with $\boldsymbol{K} = \operatorname{diag} \beta_1, \ldots, \beta_n = \boldsymbol{M}$ symmetric and positive definite. Furthermore, due to the pointwise symmetry of $\psi_i(\Delta U_i)$ we have $\boldsymbol{\mu} = \boldsymbol{\psi}(-\boldsymbol{\sigma}) = -\boldsymbol{\psi}(\boldsymbol{\sigma})$ for the input in (3b). Finally, if $\boldsymbol{I} + \boldsymbol{M}\tilde{\boldsymbol{G}}(s)$ is strictly positive real, we obtain stability by means of the Circle Criterion [23, Th. 7.1]. □

Hence, given the slopes $\beta_i, \ldots, \beta_n$ of all characteristics Theorem 1 allows for a straight-forward SA of a network since the strict positive realness condition (SPRC) can be easily verified by the criterion presented in [34].

B. Application of the Criterion

Theorem 1 only verifies the stability of a network for a given set of slopes $\beta_i,\ i = 1, \ldots, n$. In practice however, one is often interested in the actual maximal values for the slopes for which closed-loop stability can still be guaranteed. Within this contribution, two cases are considered for this problem:

a) Uniform slopes: For this case, all DERs in the network are assumed to operate with the same parameter set, yielding a uniform parameter λ for all plants such that $\beta_i = \lambda$ for $i = 1, \ldots, n$.

b) Uniform voltage support: As the impact of reactive power provisioning differs for each DER due to variations in network topology and line parameters it can be beneficial to work with uniform settings for the actual voltage support ability. For each plant this metric is given by the product of the slope β_i with the local auto-sensitivity k_i, where $k_i,\ i = 1, \ldots, n$ is the i-th element from the main diagonal of the sensitivity matrix $\boldsymbol{K}_Q$. Hence, the actual plant slopes are given by $\beta_i = -\lambda/k_i$ for $i = 1, \ldots, n$.

For both cases, the task at hand can be written as an optimization problem in the surrogate variable λ, whose value is to be maximized while upholding the SPRC from Theorem 1. This yields the following general minimization problem

$$\begin{aligned} \min_{\lambda\in\mathbb{R}^+} \quad & \frac{1}{\lambda} \\ \text{s.t.} \quad & \boldsymbol{I} + \boldsymbol{M}\tilde{\boldsymbol{G}}(s) \text{ strictly positive real} \\ & \boldsymbol{M} = \begin{cases} \lambda \boldsymbol{I} & \text{case a)} \\ -\lambda \operatorname{diag}(1/k_i, \ldots, 1/k_n) & \text{case b)} \end{cases} \end{aligned} \tag{5}$$

which is to be solved.

V. Time Series based Stability Assessment Using Wavelet Transform

In addition to analytical evaluation, the objective of this section is the comparative evaluation of time histories from either simulations or measurements. Here, the introduced DER models can be used for investigation of RMS time domain simulations in network calculation programs. The challenge consists in the automated determination of signal patterns and superimposed oscillations from signal sequences that may be affected by noise. Therefore, in the following, the authors revisit the wavelet transform as a technique for time-frequency analysis of waveforms. Based on this, the application is discussed using exemplary voltage time series.

A. The Concept of Wavelet Transformation in Respect to Power System Applications

An established approach in signal processing is the Fourier transform, which can be taken to express any signal by an infinite series of sine and cosine curves. Its major drawback is that it provides only frequency resolution, i. e., one can identify all frequencies that exist in the signal, but not their temporal occurrence. This can be remedied by using sliding evaluation windows, although these have practical limitations [35]. The wavelet transform, on the other hand, uses a fully scalable modulated window that provides a principled solution to the problem of selecting the window function [36]. The window is moved over the signal and a spectrum is computed for each position. Then the scheme is repeated for a large number of scales to obtain a signal representation with multiple time-frequency resolutions. This provides both good time resolution for high-frequency signals and good frequency resolution for low-frequency signals.

Due to the successful use in time-frequency analysis [37], [38], we chose the continuous wavelet transform (CWT). The CWT can be written in the time domain as

$$\mathcal{W}_\Upsilon[f](s,\tau) \coloneqq \frac{1}{\sqrt{|s|}} \int_{-\infty}^{\infty} \Upsilon\left(\frac{t-\tau}{s}\right) f(t)\,\mathrm{d}t, \tag{6}$$

where s is the scale factor, τ is the translation factor, $\Upsilon(t)$ is the mother wavelet to choose and $f(t)$ is the time series to transform. Here, the choice of the Morse wavelet[3] as

[3]In [22, Eq. (9)], the general Morse wavelet is expressed in the frequency domain. In this contribution, we rely on the default values for the parameter of symmetry $\gamma = 3$ and compactness $\beta = 20$.

the mother wavelet shows promise, as also be seen in the broad application in engineering disciplines [22] as well as the specific application in electrical re-balancing after network islanding [39] or after faults in hybrid AC/DC microgrids [40].

B. Application of Wavelet Transform to RMS Time Series

By analyzing the RMS histories of relevant magnitudes such as nodal voltage or plant reactive power after a small-signal excitation or during long-term measurements, one can check retroactively for undesired behavior. Here, a suitable evaluation factor is the amplitude of possibly occurring oscillatory disturbances. To do so, one can define a threshold above which the oscillation magnitude is classified as inadmissible in the form of

$$\delta = \min\{U_{\text{crit}}, u_{\text{crit}} \cdot U_{\text{nom}}\}, \tag{7}$$

where U_{crit} is a voltage level independent upper limit and u_{crit} is a factor relative to U_{nom}, which is the nominal line-to-line voltage of the node. Furthermore, for the delimitation of transient processes, a time span T_{crit} is specified, for which at least δ must be exceeded. The concrete threshold δ and the critical time span T_{crit} ought to be set by the DSO, e. g. based on the accuracy of the voltage measurement. In the following, two exemplary voltage time series depicted in Fig. 5 and Fig. 6 are discussed. In respect to (7), the threshold parameters are set to $U_{\text{crit}} = 300\,\text{V}$, $u_{\text{crit}} = 0.5\,\%$ and $T_{\text{crit}} = 2\,\text{s}$.

First, a synthetic $110\,\text{kV}$ benchmark network was parameterized with a penetration rate of $Q(V)$-controlled DERs of $100\,\%$ and the DERs were parameterized with a $Q(V)$-characteristic slope $m = 60\,\%/\text{pu}$ to cause oscillations. The system was simulated for $10\,\text{s}$ and as the event of excitation the $Q(V)$-control was activated at $t = 0\,\text{s}$. In Fig. 5 (a) a voltage oscillation with a constant frequency and magnitude is evident after the initial system response vanishes. The results of the wavelet transform are presented in Fig. 5 (b) and show frequency components of the signal that decay within the first two seconds as well as signal parts that oscillate continuously from $t \approx 2\,\text{s}$ with a magnitude up to $450\,\text{V}$. As can be seen in the lower part of Fig. 5 (a), a critical threshold violation was detected from the first time the critical evaluation time $T_{\text{crit}} = 2\,\text{s}$ was reached. The triggered critical frequency components of the RMS signal ranges from $0.59\,\text{Hz}$ to $0.84\,\text{Hz}$ and are color-coded. Note that the triggers for the different frequency components are not continuously active, but that at least one trigger is always present during the entire evaluation time.

Second, a $100\,\text{s}$ long history was selected from a measurement of a WF captured at the $21\,\text{kV}$ PCC. Figure 6 (a) shows superimposed voltage oscillations with variable magnitudes. The evaluation of the wavelet analysis in Fig. 6 (b) shows a continuous threshold violation for frequencies between $0.127\,\text{Hz}$ to $0.18\,\text{Hz}$ and period lengths of $5.5\,\text{s}$ to $7.8\,\text{s}$, respectively. Note that the usability for measurement based time series is strongly influenced by the averaging interval of the RMS measurements. A longer averaging time may mask higher frequency oscillations.

With help of the wavelet transform time-critical threshold violations could be identified for individual frequencies in both

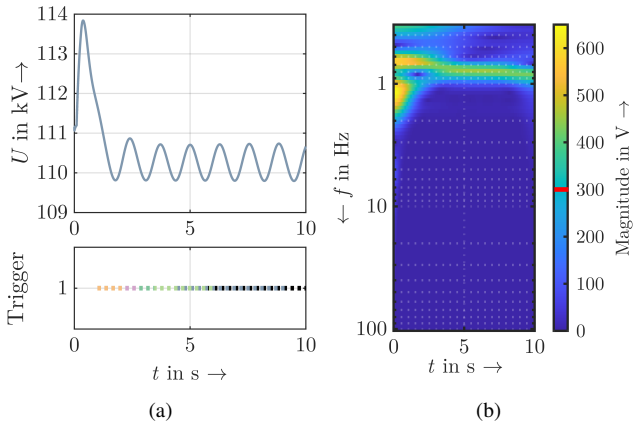

Fig. 5. Comparison of wave form and wavelet scalogram for nodal voltage on the example of a synthetic $110\,\text{kV}$ network and a sampling rate of $1000\,\text{Hz}$. (a) RMS signal (upper) and threshold trigger for different frequency components (lower). (b) Wavelet scalogram with threshold δ (red line).

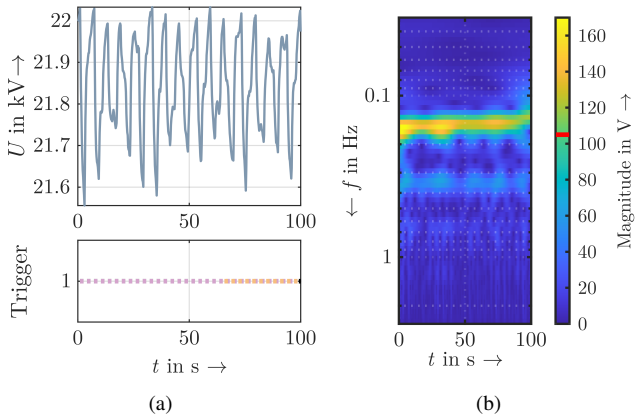

Fig. 6. Comparison of wave form and wavelet scalogram for nodal voltage on the example of a measured $21\,\text{kV}$ network and a sampling rate of $5\,\text{Hz}$. (a) RMS signal (upper) and threshold trigger for different frequency components (lower). (b) Wavelet scalogram with threshold δ (red line).

example histories. To better distinguish between permissible and impermissible signal patterns, one can fine-tune the mother wavelet or adjust the evaluation time window for simulations in which the disturbance is known. The presented postponed assessment of voltage time series will be used in the next section for the automatic evaluation of power system simulations.

VI. Verification of Stability Assessment Criteria

The stability criterion, introduced in Section IV, is applied to four different HV networks. The authors provide general advices for the practical application. Subsequently, a comparison with the criterion introduced in [19] and stability bounds based on RMS simulations utilizing the wavelet assessment from Section V is carried out. The type WF-FRC according to Table III is used as DER model.

A. Benchmark networks

Four HV networks, two synthetic ones (sDN) and two realistic ones (rDN), are used for benchmarking purposes. All benchmark networks were parameterized with $100\,\%$ of the

rated power of the consumer and generator loads. The sDN1 was introduced in [13], [19] and is characterized by a $100\,\%$ penetration rate of $Q(V)$-controlled nodes. The development of sDN2 was based on realistic network data from Germany within the *SimBench* project [25]. Here, the variant *Mixed* has been modified by replacing the transformers of the network interconnection points with overhead line equivalents fed to a common $110\,\mathrm{kV}$ slack. Furthermore, all generators with a rated power greater than $1\,\mathrm{MW}$ were equipped with a $Q(V)$-control. Both rDN are based on real topology data, but information on the control structures is missing. They are located in the area of transmission system operator in the eastern part of Germany *50Hertz Transmission GmbH* and thereby represent different DER penetration rates. Due to this, the DER penetration factor ρ is introduced to further make these networks comparable in respect to their DER penetration:

$$\rho = \frac{\sum P_{\text{DER inst}}}{\ell_{\text{DN}}}. \tag{8}$$

Herein, $P_{\text{DER inst}}$ is the installed active power of a DER unit and ℓ_{DN} is the cumulative branch length of the related DN. As a reference, the average penetration factor for whole Germany in the year 2021 is $\rho_{\text{GER}} \approx 60\,\mathrm{kW/km}$. It is to mention that rural DNs usually have a higher DER penetration than urban DNs. Table I summarizes the key characteristics of the benchmark networks. In general, ρ is significantly lower for realistic DNs than for the synthetic ones with DER focus. Nonetheless, additional evaluations have shown that there are also DNs within the area of the transmission system operator where ρ is above $1000\,\mathrm{kW/km}$.

B. Application procedure

The aforementioned power systems have been implemented in `PowerFactory` and all DERs were replaced by detailed DER models of the type WF-FRC, c. f. Table III, and equipped with a $Q(V)$-control. Further, it holds: (i) each DER has the same slope m, (ii) the $Q(V)$-characteristics contain no dead band, i. e. $\beta = m$[4]. For all procedures of SA, the maximum admissible slope β is obtained by means of (5) case a).

As a reference, RMS simulations were performed in `PowerFactory`. After a small signal disturbance, the nodal voltage responses were recorded for a duration of $15\,\mathrm{s}$ and evaluated using the wavelet transform based on Section V. Hereby, the cause of a disturbance can be a ramp or step in active power infeed of DERs, a step in the transformer ratio or voltage level respectively as well as a failure of a network asset. For simplification of evaluation, the active power feed-in of all DERs was increased ramp-like for the first $5\,\mathrm{s}$. To be classified as stable, a nodal voltage oscillation must not violate the threshold $\delta = \min\{300\,\mathrm{V}, 0.5\,\% \cdot U_{\text{nom}}\}$ for a set duration $T_{\text{crit}} = 1\,\mathrm{s}$ at the end of the evaluation window. Thus, it has to show a significant decay within $10\,\mathrm{s}$ after the disturbance event.

In addition, the analytical SA predominantly relies on the topology and the operating point of the network. Therefore, an automatic export of the network data provided in `PowerFactory` to an interoperable JSON based power system data model [41] is executed using the open source toolbox *powerfactory-tools* [42]. Subsequently, the nodal voltage sensitivities $\boldsymbol{K}_Q$ are computed as required to build the linear transfer function matrix $\tilde{\boldsymbol{G}}(s)$ as in (3). Applying the presented Circle Criterion in (5), a critical slope β can be found.

In general, DSOs are enabled to assess their network configuration regarding *converter-driven stability* in respect to available information. Analytical approaches provide a reliable, fast, but conservative SA and can be easily adapted to different network operating points. If the DSO requires increasing the $Q(V)$ slopes beyond the calculated limits or performing cross-validation, the presented simulative approach using the wavelet transform allows an automatable SA and provides less conservative results. Table II provides a brief summary of applicable methods.

C. Discussion of Stability Assessment Results

A SA was carried out for the introduced benchmark networks. Figure 7 displays the comparison of the results for the SA introduced in Section IV (Circle) with the method presented in the previous study [19] (Robust) and reference evaluations based on simulated time series in `PowerFactory`, utilizing the automatic wavelet SA (Wavelet). In addition, the Circle and Robust criterion were applied for the PT_2 plant models.

The maximum allowable slopes vary across the benchmark networks, as expected due to the differences in network structure and DER penetration. On the other hand, the trend of the results with respect to the the selected DER models and the criteria is the same for all networks. It is confirmed that

TABLE I
OVERVIEW OF BENCHMARK NETWORK CHARACTERISTICS.

Distribution network	CPs to 380 kV	No. of Nodes	$\sum P_{\text{DER}}$ in MW	ρ in kW/km
sDN1	2	50	480	1400
sDN2	3	61	1560	1400
rDN1	2	65	135	$\approx 400^*$
rDN2	3	210	840	$\approx 600^*$

* As concrete branch length of network is unavailable, ρ of related DSO network area is presented instead.

[4]If a dead band is assumed, the $Q(V)$-characteristic slope m is higher than the enclosing slope of the nonlinearity sector β, but limited through the maximum reactive power Q_{max}, see Fig. 3. This does not affect the applicability of the presented criterion.

TABLE II
OVERVIEW OF THE APPLICATION OF THE SA CRITERIA RELATED TO THE KNOWLEDGE OF DER MODELS.

SA class	Knowledge of DER plant model		
	None	Blackbox	Whitebox
Analytical	Robust with PT_2-TAR	Robust with PT_2-DER	Robust
	Circle with PT_2-TAR	Circle with PT_2-DER	Circle
Simulatory	-	Wavelet	Wavelet

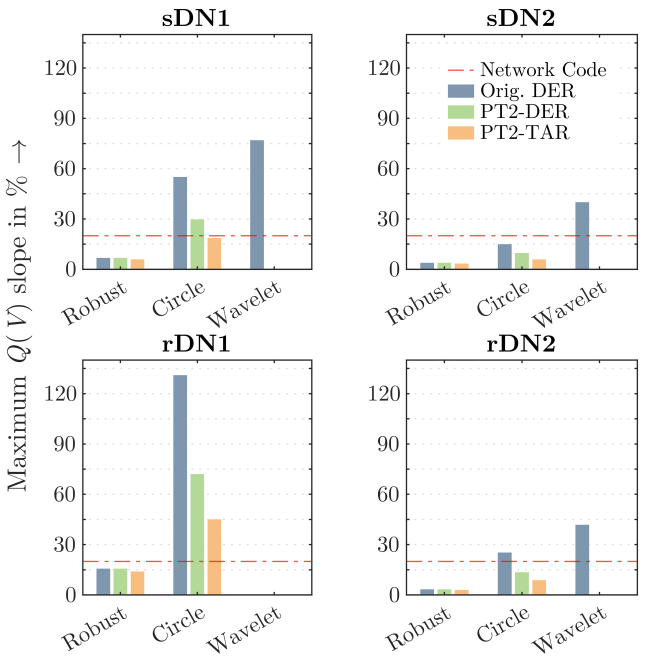

Fig. 7. Maximum admissible $Q(V)$ slopes as results of the SA (Robust, Circle, Wavelet). Three different DER models were implemented in each of the four HV benchmark networks. Only Orig. DER model is simulated in PF ref. No limitation could be detected in rDN1 due to insufficient reactive power resources.

with better knowledge of the DER parameterization, a higher slope can be considered acceptable. Furthermore, the results of the most robust criterion are always the most conservative, followed at a considerable distance by the Circle criterion. The SA based on the wavelet transform results in stability limits that are substantially higher than the robust and Circle criteria for all benchmark networks. In addition, they are above the recommendation given in the network code [33], which is $m = 6\,\%/\mathrm{pu}$ to $20\,\%/\mathrm{pu}$. Except for sDN2, the results of the Circle criterion are also above this recommended limit.

Applying only the robust criterion to different DER representations, PT_2-TAR leads to worse results, due to a higher closed loop gain that is being assumed[5]. Utilizing the Circle Criterion instead, a higher stability limit can be guaranteed, regardless of the DER representation. As example, Fig. 7 shows for sDN1 a stability limit of $18.6\,\%/\mathrm{pu}$ (Circle, PT_2-TAR) against $6.8\,\%/\mathrm{pu}$ (Robust, PT_2-TAR). Furthermore, it can be stated that the result using the original DER transfer functions is the less conservative one. This effect follows from the conservative simplification steps. Utilizing the PT_2-DER approximation, the results are significantly better than with PT_2-TAR. This is not surprising as the PT_2-TAR model represents the worst DER that is still allowed within the TAR specifications, where the PT_2-DER tries to approximate the actual DER dynamics.

As conclusion for the PT_2 control loop simplifications, the PT_2-DER offers a shorter computing time in comparison to Orig. DER due to the reduced model complexity and the PT_2-TAR allows the application even without knowledge of the control loop parameterization. As a trade-off for broader applicability, the results are generally more conservative than those using the detailed DER model.

[5]For PT_2-TAR approximation a worst case overshoot of $\xi = 15\,\%$ is set, instead the maximum closed loop gain for a broad range of parameterization is assumed as 1 for Orig. DER and PT_2-DER.

VII. Conclusion

The authors present ongoing work on the evaluation of multi-input multi-output reactive power control systems in distribution networks. The work focuses on the interdependent $Q(V)$-characteristic voltage control. Subsequently, an analytical method for stability assessment based on the Circle Criterion was introduced. The new method enables the computation of a guaranteed stability limit for the $Q(V)$-characteristic slope taking into account the parameters of the DER plant model. The input variables required are the node admittance matrix, the network operating point, and the DER mode As an alternative, PT_2 approximations of DER plant models can be used instead. In addition, a procedure based on the wavelet transform was presented to evaluate RMS time series and make these results comparable to the analytical assessment.

The stability assessment methods were applied to four different high-voltage benchmark networks. The results show a higher guaranteed stability limit compared to the previous work [19] as well as the TAR recommendations. A significant advantage over RMS simulations performed in `PowerFactory` is that the analytic evaluation is considerably faster and does not require implemented plant models in a network calculation program. The disadvantage is the conservative nature of the Circle criterion. Nonetheless, the presented work can be used to support network-wide equipment of DERs with a $Q(V)$-characteristic based voltage control in distribution networks with a high DER penetration. Furthermore, the secure application of a distributed $Q(V)$ fallback control for a centralized network-wide setpoint-based voltage control is conceivable as presented in [5].

Future work will focus on fine-tuning of the Morse mother wavelet, additional assessment criteria, and diverse network modeling. It is planned to adopt other approaches, such as [43], [44], for the stability assessment of nonlinear systems. The conservative nature of the presented criterion should be compared with the assessment approach of [21], [45] in the time-discrete domain. As part of a concluding benchmark, the Nyquist method will also be used for a linearly assumed MIMO system. Also, as presented in [20], a better representation of the voltage-dependent nodal sensitivities by using sensitivity gradients is possible, but sophisticated since it adds an additional nonlinearity. In contrast, the more direct approach is to use a static network model, see [46]. However, to take advantage of this modeling approach, the voltage support must be implemented via an $I(U)$-characteristic instead of a $Q(V)$-characteristic. This progressive approach also opens up new possibilities for stability evaluation.

Acknowledgments

This research was founded by the Deutsche Forschungsgemeinschaft (DFG, DOI: 10.13039/501100001659) – project no. 442893506.

The Article Processing Charge (APC) was funded by the joint publication funds of the TU Dresden, including Carl Gustav Carus Faculty of Medicine, and the SLUB Dresden as well as the Open Access Publication Funding of the DFG.

REFERENCES

[1] S. Krahmer, S. Ecklebe, P. Schegner, and K. Röbenack, "Analysis of the Converter-Driven Stability of Q(V)-Characteristic Control in Distribution Grids," in *SEST 2022 - 5th International Conference on Smart Energy Systems and Technologies*. IEEE, 2022.

[2] M. Zhao, X. Yuan, J. Hu, and Y. Yan, "Voltage Dynamics of Current Control Time-Scale in a VSC-Connected Weak Grid," *IEEE Trans. Power Syst.*, vol. 31, no. 4, pp. 2925–2937, 2016.

[3] M. Chiandone, R. Campaner, V. Arcidiacono, G. Sulligoi, and F. Milano, "Automatic voltage and reactive power regulator for wind farms participating to TSO voltage regulation," in *2015 IEEE Eindhoven PowerTech*, 2015.

[4] O. Marggraf and B. Engel, "Experimental and Field Tests of Autonomous Voltage Control in German Distribution Grids," in *2018 IEEE PES Innovative Smart Grid Technologies Conference Europe (ISGT-Europe)*, 2018.

[5] F. Thomas, S. Krahmer, and P. Schegner, "Robust and Optimized Voltage Droop Control considering the Voltage Error," in *IEEE Power and Energy Student Summit (PESS) 2019*, 2019. [Online]. Available: https://doi.org/10.13140/RG.2.2.13647.23208

[6] A. Inaolaji, A. Savasci, and S. Paudyal, "Distribution Grid Optimal Power Flow in Unbalanced Multiphase Networks With Volt-VAr and Volt-Watt Droop Settings of Smart Inverters," *IEEE Transactions on Industry Applications*, vol. 58, no. 5, pp. 5832–5843, 2022.

[7] N. Hatziargyriou, J. Milanovic, C. Rahmann, V. Ajjarapu, C. Canizares, I. Erlich, D. Hill, I. Hiskens, I. Kamwa, B. Pal, P. Pourbeik, J. Sanchez-Gasca, A. Stankovic, T. Van Cutsem, V. Vittal, and C. Vournas, "Definition and classification of power system stability - revisited & extended," *IEEE Trans. Power Syst.*, vol. 36, no. 4, pp. 3271–3281, Jul. 2021.

[8] European Union, "Commission Regulation (Eu) 2016/631 Establishing a Network Code on Requirements for Grid Connection of Generators (RFG)," *Official Journal of the European Union*, no. 14 April 2016, p. 68, 2016. [Online]. Available: https://op.europa.eu/en/publication-detail/-/publication/1267e3d1-0c3f-11e6-ba9a-01aa75ed71a1/language-en

[9] F. Andren, B. Bletterie, S. Kadam, P. Kotsampopoulos, and C. Bucher, "On the Stability of Local Voltage Control in Distribution Networks With a High Penetration of Inverter-Based Generation," *IEEE Trans. Ind. Electron.*, vol. 62, no. 4, pp. 2519–2529, April 2015.

[10] M. Lindner and R. Witzmann, "On the stability of Q(V) in distribution grids," in *IEEE PES Innovative Smart Grid Technologies Conference Europe*, 2018.

[11] F. Hans and W. Schumacher, "Modeling and Small-Signal Stability Analysis of Decentralized Energy Sources implementing Q(U) Reactive Power Control," in *11th IEEE International Conference on Compatibility, Power Electronics and Power Engineering (CPE-POWERENG)*, 2017, pp. 588–593.

[12] J. H. Braslavsky, L. D. Collins, and J. K. Ward, "Voltage Stability in a Grid-Connected Inverter with Automatic Volt-Watt and Volt-VAR Functions," *IEEE Trans. Smart Grid*, vol. 10, no. 1, pp. 84–94, 2019.

[13] M. Kreutziger, P. Schegner, S. Wende-von Berg, and M. Braun, "Reactive Power Management of Distributed Generators for Selective Voltage Optimization in 110-kV-Subtransmission Grids," in *Conference on Sustainable Energy Supply and Energy Storage Systems (NEIS 2018)*, Hamburg, Germany, 2018.

[14] S. Asadollah, R. Zhu, and M. Liserre, "Analysis of voltage control strategies for wind farms," *IEEE Trans. Sustainable Energy*, vol. 11, no. 2, pp. 1002–1012, 2020.

[15] M. Hau and M. Shan, "Stability of Fast Q(U) Voltage Droop Control of Wind Parks in High Voltage Distribution Grids Reduced Model of the Wind Park Voltage Control System," in *NEIS 2017 Conference on Sustainable Energy Supply and Energy Storage Systems*, Hamburg, 2017.

[16] Y. Qian, X. Yuan, and M. Zhao, "Analysis of voltage control interactions and dynamic voltage stability in multiple wind farms," in *IEEE Power and Energy Society General Meeting*, Boston, USA, 2016.

[17] B. Heimbach, M. Mangani, B. Wartmann, M. Oeschger, C. Kelm, S. Krahmer, M. Kreutziger, and P. Schegner, "Contribution of a wind farm to voltage and system stability: results of a measurement campaign," *CIRED Open Access Proc. J.*, vol. 2017, pp. 1646–1649, October 2017.

[18] A. Eggli, S. Karagiannopoulos, S. Bolognani, and G. Hug, "Stability analysis and design of local control schemes in active distribution grids," *IEEE Trans. Power Syst.*, vol. 36, no. 3, pp. 1900–1909, 2021.

[19] S. Krahmer, A. Saciak, J. Winkler, P. Schegner, and K. Robenack, "On robust stability criteria for nonlinear voltage controllers in electrical supply networks," in *2018 Power Systems Computation Conference (PSCC)*, 2018.

[20] F. Thomas, S. Krahmer, J. Winkler, P. Schegner, and K. Röbenack, "On Grid Modeling for Stability Assessment of Droop Voltage Control," in

TABLE III
PROPOSED MODEL CONFIGURATION OF DIFFERENT DER TYPES AND RELATED PT_2 APPROXIMATIONS.

DER type	Control loop $G(s)$: Voltage averaging	Control loop $G(s)$: Reactive power control loop	Ref.
(i) WF-FRC	$\frac{1}{1+sT_\mathrm{U}}$, $T_\mathrm{U}=0.02\,\mathrm{s}$	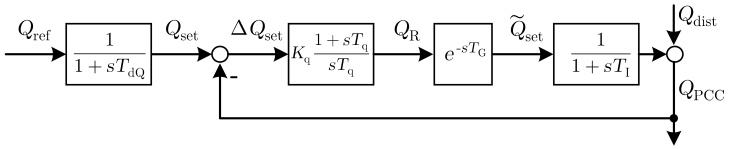 $T_\mathrm{dQ}=2\,\mathrm{s}$, $K_\mathrm{q}=0.5$, $T_\mathrm{q}=0.2\,\mathrm{s}$, $T_\mathrm{I}=0.1\,\mathrm{s}$, $T_\mathrm{g}=0.2\,\mathrm{s}$	[19], [29], [47]
(ii) WF-DFIG		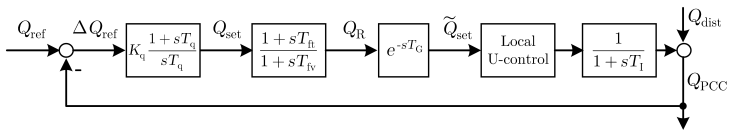	[19], [27], [47]
(iii) WF-DFIG	$\frac{1}{(1+sT_\mathrm{U})^3}$, $T_\mathrm{U}\approx 0.004\,\mathrm{s}$	A PV inverter with fast power control settings (cf. T_I in [30]) extended by a farm control. The emerging control loop can be established analogously to (i) with $T_\mathrm{dQ}=2\,\mathrm{s}$, $K_\mathrm{q}=0.5$, $T_\mathrm{q}=0.2\,\mathrm{s}$, $T_\mathrm{I}=0.0033\,\mathrm{s}$, $T_\mathrm{g}=0.1\,\mathrm{s}$.	[30]
(iv) PT_2-TAR	Not necessary	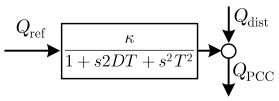	Based on the generic step response given in TAR with $\kappa=1$, $D=0.517$, $T=2.335\,\mathrm{s}$.	[33]
(v) PT_2-DER			Based on the frequency response of detailed DER model (i) with $\kappa=1$, $D=0.747$, $T=1.028\,\mathrm{s}$.	

2019 IEEE PES Innovative Smart Grid Technologies Conference Europe (ISGT-Europe), 2019.
[21] J. Schmitt, S. Ecklebe, and S. Krahmer, "An extended stability criterion for grids with Q(V)-controlled distributed energy resources," Jun. 2023, unpublished, submitted to IEEE Power and Energy Student Summit (PESS) 2023. [Online]. Available: https://doi.org/10.36227/techrxiv.23853369.v1
[22] E. A. Martinez-Ríos, R. Bustamante-Bello, S. Navarro-Tuch, and H. Perez-Meana, "Applications of the generalized morse wavelets: A review," *IEEE Access*, vol. 11, pp. 667–688, 2023.
[23] H. K. Khalil, *Nonlinear Systems*, 3rd ed. Upper Sadle River, NJ: Prentice-Hall, 2002.
[24] S. Krahmer. Application of Stability Analysis of Q(V)-Characteristic Controls Related to the Converter-Driven Stability in Distribution Networks [Source Code]. Code Ocean Capsule.
[25] S. Meinecke, D. Sarajlić, S. R. Drauz, A. Klettke, L. P. Lauven, C. Rehtanz, A. Moser, and M. Braun, "SimBench-A benchmark dataset of electric power systems to compare innovative solutions based on power flow analysis," *Energies*, vol. 13, no. 12, 2020.
[26] K. O. Papailiou, Ed., *Springer Handbook of Power Systems*. Singapore: Springer, 2021.
[27] J. M. Garcia, "Voltage control in wind power plants with doubly fed generators," Dissertation, Aalborg University, 2010.
[28] J. Fortmann, *Modeling of Wind Turbines with Doubly Fed Generator System*. Wiesbaden: Springer Fachmedien Wiesbaden, 2015.
[29] IEC 61400-27-1:2020, "Wind energy generation systems - Part 27-1: Electrical simulation models - Generic models," 2020.
[30] M. Lindner and R. Witzmann, "Modelling and validation of an inverter featuring local voltage control Q(V) for transient stability and interaction analyses," *Int. J. Electr. Power Energy Syst.*, vol. 101, no. March, pp. 280–288, 2018.
[31] M. Eremia, C.-C. Liu, and A.-A. Edris, "Static VAr Compensator (SVC)," in *Advanced Solutions in Power Systems: HVDC, FACTS, and Artificial Intelligence*. Wiley-IEEE Press, 2016, pp. 271–338.
[32] R. I. Cabadag, "Analysis of the Impact of Reactive Power Control on Voltage Stability in Transmission Grids," Dissertation, Technische Universität Dresden, 2019.
[33] VDE-AR-N 4120:2018-11, "Technical requirements for the connection and operation of customer installations to the high voltage network (TAR high voltage)," 2018.
[34] R. Shorten, P. Curran, K. Wulff, C. King, and E. Zeheb, "On spectral conditions for positive realness of transfer function matrices," *Proceedings of the American Control Conference*, vol. 53, no. 5, pp. 1076–1079, 2008.
[35] A. Bonami, B. Demange, and P. Jaming, "Hermite functions and uncertainty principles for the Fourier and the windowed Fourier transforms," *Rev. Mat. Iberoam.*, vol. 19, no. 1, pp. 23–25, 2003.
[36] C. Valens, "A really friendy guide to wavelets," Department of Computer Science, The University of NewMexico, Tech. Rep., 1999. [Online]. Available: https://cs.unm.edu/~williams/cs530/arfgtw.pdf
[37] B. Boashash, *Time Frequency Signal Analysis and Processing: A Comprehensive Reference*. Elsevier, 2016.
[38] I. Kiskin, D. Zilli, Y. Li, M. Sinka, K. Willis, and S. Roberts, "Bioacoustic detection with wavelet-conditioned convolutional neural networks," *Neural Computing and Applications*, vol. 32, pp. 915–927, 2020.
[39] O. A. Allan and W. G. Morsi, "A new passive islanding detection approach using wavelets and deep learning for grid-connected photovoltaic systems," *Electr. Power Syst. Res.*, vol. 199, p. 107437, 2021.
[40] Y. Seyedi, J. Mahseredjian, and H. Karimi, "Impact of fault impedance and duration on transient response of hybrid ac/dc microgrid," *Electr. Power Syst. Res.*, vol. 197, p. 107298, 2021.
[41] Power System Data Model - A data model for the description of electrical power systems. Python Package. Institute of Electrical Power Systems and High Voltage Engineering - TU Dresden.
[42] PowerFactory Tools - A toolbox for Python based control of DIgSILENT PowerFactory. Python Package. Institute of Electrical Power Systems and High Voltage Engineering - TU Dresden.
[43] M. G. Safonov, "Stability of interconnected systems having slope-bounded nonlinearities," in *Analysis and Optimization of Systems. Lecture Notes in Control and Information Sciences,*, A. Bensoussan and J. e. Lions, Eds. Springer, Berlin, Heidelberg, 2005, vol. 62, pp. 275 – 287. [Online]. Available: https://link.springer.com/chapter/10.1007/BFb0004960
[44] I. Lestas and G. Vinnicombe, "Scalable decentralized robust Stability certificates for networks of interconnected heterogeneous dynamical systems," *IEEE Trans. Autom. Control*, vol. 51, no. 10, pp. 1613–1625, 2006.
[45] R. H. Gielen and M. Lazar, "On stability analysis methods for large-scale discrete-time systems," *Automatica*, vol. 55, pp. 66–72, 2015.
[46] S. Ecklebe, S. Krahmer, and K. Robenack, "A Time-Based Approach to the Modelling of Power Distribution Grids," in *25th International Conference on System Theory, Control and Computing (ICSTCC 2021)*, Iasi, Romania, 2021, pp. 425–430.
[47] WECC Modeling and Validation Work Group, "WECC Wind Plant Dynamic Modeling Guidelines," Western Electricity Coordinating Council (WECC), Tech. Rep., 2014. [Online]. Available: http://www.wecc.biz/committees/StandingCommittees/PCC/TSS/MV

Sebastian Krahmer Dipl.-Ing. Sebastian Krahmer is a research associate at the Institute of Electrical Power Supply and High Voltage Engineering at TUD Dresden University of Technology. Since 2019, he has been group leader of the Planning and Operation of Grids working group. His research interests are the design of operation management concepts including modern communication standards, the contribution of distributed generation plants to system services, related stability assessment methods and DC microgrids.

Stefan Ecklebe Dipl.-Ing. Stefan Ecklebe is a research associate at the Institute for Control Theory at TUD Dresden University of Technology. His research interests include modeling and control of systems with locally distributed parameters in crystal growing as well as modeling and stability analysis of electrical networks with distributed generation systems.

Peter Schegner Prof. Peter Schegner is director of the Institute for Electrical Power Supply and High Voltage Technology at TUD Dresden University of Technology. He is in charge of numerous research projects in the fields of: Planning and operation of electrical networks, quality of supply, design and operation of smart grids, selective protection and automation technology, and stability of electrical network.

Klaus Röbenack Prof. Klaus Röbenack is Director of the Institute for Control Theory at the Faculty of Electrical Engineering and Information Technology at TUD Dresden University of Technology. His fields of work include the design of nonlinear controllers and observers and scientific computing.